AD-A090 802 SCIENTIFIC RESEARCH ASSOCIATES INC GLASTONBURY CT F/G 20/4
COMPUTATION OF THREE-DIMENSIONAL HORSESHOE VORTEX FLOW USING TH--ETC(U)
1980 W R BRILEY, H MCDONALD N00014-77-C-0075

UNCLASSIFIED NL

1 OF 1
AD A090802

END
DATE FILMED
11-80
DTIC

LEVEL II

COMPUTATION OF THREE-DIMENSIONAL HORSESHOE VORTEX FLOW USING THE NAVIER-STOKES EQUATIONS

Contract N00014-77-C-0075

W. Roger Briley and Henry McDonald
Scientific Research Associates, Inc.
P.O. Box 498, Glastonbury, CT 06033

Presented at the Seventh International Conference on Numerical Methods in Fluid Dynamics,
Stanford University and NASA/Ames, June 23-27, 1980.

COMPUTATION OF THREE-DIMENSIONAL HORSESHOE VORTEX FLOW USING THE NAVIER-STOKES EQUATIONS

W. R. Briley and H. McDonald
Scientific Research Associates, Inc.
P.O. Box 498, Glastonbury, CT 06033

ABSTRACT

Numerical solutions of the compressible Navier-Stokes equations are presented for a laminar horseshoe vortex flow created by the interaction of a boundary layer on a flat surface and an elliptical strut leading edge mounted normal to the flat surface. The computational approach utilizes "zone embedding", surface-oriented elliptic-cylindrical coordinates, interactive boundary conditions, and a consistently-split linearized block implicit (LBI) scheme developed by the authors. Mesh resolution tests are performed, and the horseshoe vortex flow is discussed.

INTRODUCTION

The present study considers three-dimensional leading-edge horseshoe vortex flow representing the interaction of a two-dimensional wall boundary layer approaching an elliptical strut leading edge mounted normal to a flat surface. An example of this type of flow occurs near the junction of an airfoil or wing and its supporting surface. Another example is present in axial compressors and turbines, where boundary layers which develop on the annular surfaces of the axial flow passage encounter rows of stationary and rotating blades. The flow is of interest in connection with flow degradation, its tendency to cause high local heat transfer rates, and its role as the origin of corner flows. Numerous experimental flow visualization studies (e.g., [1-3]) have established that the flow consists of a three-dimensional boundary layer separation in front of the obstruction followed by a vortex flow which wraps around the obstruction. Little is available in the way of detailed flow measurements, however, particularly downstream of separation. Previous analytical studies have considered the three-dimensional boundary layer flow upstream of separation (e.g., [4]) and have used rotational inviscid flow theory to estimate secondary flows [5]. The horseshoe vortex flow is treated here by numerical solution of the compressible Navier-Stokes equations for laminar flow at moderate Reynolds number Re and low Mach number M. The study has as its goals an improved understanding of the horseshoe vortex region and formation of corner flows, and also the development of flow prediction techniques.

ZONE EMBEDDING AND INTERACTIVE BOUNDARY CONDITIONS

The compressible Navier-Stokes equations in general orthogonal coordinates are solved using analytical coordinate data for an elliptic-cylindrical coordinate system which fits all solid surfaces within the computational domain but is not aligned with the direction of the free stream flow. In selecting the computational domain, a "zone embedding" approach is adopted whereby attention is focused on a subregion of the overall flow field in the immediate vicinity of the leading edge horseshoe vortex flow. A perspective view of the geometry, coordinate system (ξ,η,z) and a representative computational grid is shown in Fig. 1. The elliptic coordinates ξ,η are related to Cartesian coordinates x,y by $x=\cosh\xi\cos\eta$, $y=\sinh\xi\sin\eta$, and the (conformal) metric scale factor h is given by $h^2=\cosh^2\xi-\cos^2\eta$. The computational domain is defined by $0.2\le\xi\le1.6$, $\pi/2\le\eta\le3\pi/2$, $0\le z\le1$.

Symmetry conditions are applied at z=1, so that the flow represented is that past an elliptical cylinder (of major semi-axis a=1.02 and minor semi-axis b=0.2) between parallel flat plates with spacing H=2. Velocity boundary conditions at no-slip and symmetry surfaces are straightforward and self-explanatory. The remaining condition applied at these boundaries is $\partial p/\partial n=0$, where p is pressure and n denotes the normal coordinate direction. The condition $\partial p/\partial n=0$ at a no-slip surface is cor-

rect to order Re^{-1} for viscous flow at high Reynolds number.

The treatment of inflow and outflow conditions is the principal obstacle to be overcome within the present zone embedding approach. At curved boundaries located within the free stream region, interactive boundary conditions are derived from an assumed flow structure and physical approximations which permit inflow of a boundary layer and inviscid free stream, and which permit outflow in the presence of shear layers, corner flow, streamwise vorticity and a nonuniform free stream. The initial conditions and interactive boundary conditions are devised from the incompressible potential flow velocity $\bar{U}_I(\xi,\eta)$ about the ellipse, together with two-dimensional estimates of the boundary layer thicknesses on the endwall flat plate, $\delta_1(x)$, and on the ellipse, $\delta_2(\eta)$, and finally from an estimate of the blockage correction factor B(x) for the core flow velocity due to the endwall boundary layer growth. The complex potential W for flow past an ellipse at incidence α with circulation k is given by Milne-Thomson [6] as $W=U_r(a+b)\cosh(\zeta-\xi_o-i\alpha)$, where U_r is a reference free stream velocity, $\xi=\xi_o$ is the ellipse surface, and ζ is defined by $x+iy=c\cosh\zeta$, where $i^2=-1$ and $c^2=a^2-b^2$. This defines the incompressible potential flow velocity $\bar{U}_I$. The boundary layer thicknesses δ_1 and δ_2 are approximated by the Blasius value $5(s/Re)^{1/2}$ where s is distance from the flat plate or ellipse leading edges, as appropriate. The blockage factor is given by $B(x)=[H/2-\delta_1^*(x)]^{-1}$. Finally, boundary layer velocity profile shapes $f_1(z/\delta_1)$ and $f_2(\xi,\delta_2)$, $0\le f_1,f_2\le 1$ are defined from vonKarman-Pohlhausen polynomial profiles. The initial velocity vector $\bar{U}$ at t=o is defined by

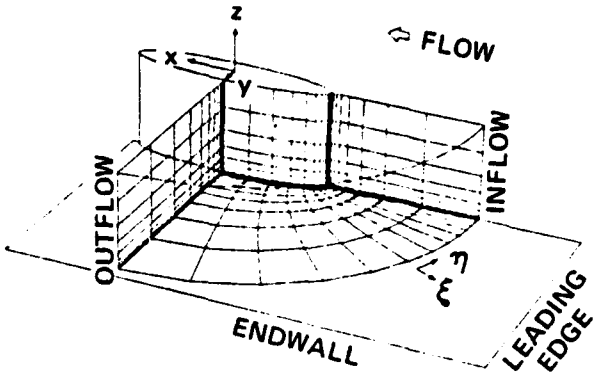

Fig. 1 - Geometry, Coordinate System, and Representative Grid

$$\bar{U}(\xi,\eta,z)=\bar{U}_I(\xi,\eta)\;B(x)\;f_1\left[z/\delta_1(x)\right]f_2\left[(\xi-\xi_0)/\delta_2(\eta)\right] \tag{1}$$

At the inflow boundary $\xi=\xi_2$, a "two-layer" boundary condition is devised such that stagnation pressure p_o is fixed at the free stream reference value $(p_o)_r$ in the core flow region ($z>\delta_1$), and the Cartesian velocity u is set by $u=u_e(\eta,t)f_1(z/\delta_1)$ for $z\le\delta_1$. Here, u_e is the local free stream velocity consistent with p_o and the local wall static pressure (assumed constant across the shear layer), which is determined as part of the solution and updated after each time step. The remaining inflow conditions are $v=\alpha U_r f_1(z/\delta_1)$, $\partial^2 w/\partial n^2=o$, and $\partial^2 c_p/\partial n^2=g(\eta,z)$ where g is the distribution of this quantity at t=o with c_p defined as $(1-B^2\bar{U}_I\cdot\bar{U}_I)$, its value from the potential flow corrected for estimated blockage. The velocities v and w are the Cartesian velocity components normal to the plane of the ellipse chord and normal to the flat plate, respectively. The angle α is the approach flow incidence angle relative to the chord of the ellipse. For outflow conditions, second normal derivatives of each Cartesian velocity component are set to zero and c_p is imposed and updated after each

time step from an interaction model relating the computed outflow velocities and the a priori potential flow solution. The imposed c_p is obtained by integrating an inviscid normal momentum equation $\partial p/\partial n=-q^2/R_I$ along the outflow symmetry lines ($z=1,\eta=\tau/2,3\pi/2$) beginning with a fixed wall pressure. Here, q is the local computed flow speed ($q^2\equiv\bar{U}\cdot\bar{U}$) and R_I is the local potential flow streamline radius of curvature. The resulting static pressure distribution is imposed at the outflow surface assuming no variation normal to the endwall.

The foregoing interactive inflow-outflow boundary conditions are designed to permit the mass flux through the computational domain to adjust to both the imposed downstream static pressure and to viscous losses present in the flow, while maintaining a specified flow structure based on physical assumptions consistent with the flow problem under consideration. Various refinements in the interactive boundary conditions are possible, such as including the effect of local pressure gradient on boundary layer growth and profile shape.

DIFFERENCING PROCEDURES

The differencing procedures used are a straightforward adaptation of those used by the authors [7] in Cartesian coordinates for flow in a straight duct. The compressible time-dependent Navier-Stokes equations are written in general orthogonal coordinates, and for economy the stagnation enthalpy is assumed constant. The definition of stagnation enthalpy and the equation of state for a perfect gas can then be used to eliminate pressure and temperature as dependent variables, and solution of the energy equation is unnecessary. The continuity and three momentum equations are solved with density and the ξ,η and z velocity components as dependent variables. Three-point central differences were used for spatial derivatives, and second-order artificial dissipation terms are added as in [7] to prevent spatial oscillations at high cell Reynolds number. This treatment lowers the formal accuracy to first order but does not seriously degrade accuracy in representing viscous terms in thin shear layers. Analytical coordinate transformations were used to redistribute grid points and thus improve resolution in shear layers and near the leading edge. Derivatives of geometric data were determined analytically for use in the difference equations.

SPLIT LBI ALGORITHM

The numerical algorithm used is the consistently-split "linearized block implicit" (LBI) scheme developed by the authors [7, 8] for systematic use in solving systems of nonlinear parabolic-hyperbolic partial differential equations (PDE's). To illustrate the algorithm, let

$$(\phi^{n+1}-\phi^n)/\Delta t = \beta D(\phi^{n+1}) + (1-\beta) D(\phi^n) \tag{2}$$

approximate a system of time-dependent nonlinear PDE's (centered about $t^n+\beta\Delta t$) for the vector ϕ of dependent variables, where D is a multidimensional vector spatial differential operator, and t is a discretized time variable such that $\Delta t=t^{n+1}-t^n$. A local time linearization (Taylor expansion about ϕ^n) is introduced, and this serves to define a linear differential operator L such that

$$D(\phi^{n+1}) = D(\phi^n) + L^n(\phi^{n+1}-\phi^n) + O(\Delta t^2) \tag{3}$$

Eq. (2) can thus be written as the linear system

$$(I-\beta\Delta t L^n)(\phi^{n+1}-\phi^n) = \Delta t D(\phi^n) \tag{4}$$

The multidimensional operator L is divided into three "one-dimensional" sub-operators $L=L_1+L_2+L_3$ (associated here with the three coordinate directions), and Eq. (4) is split as in the scalar development of Douglas & Gunn [9] and is written as

$$(I-\beta\Delta t L_1^n)(\phi^*-\phi^n) = \Delta t D(\phi^n) \tag{5a}$$

$$(I-\beta\Delta t L_2^n)(\phi^{**}-\phi^n) = \phi^*-\phi^n \tag{5b}$$

$$(I-\beta\Delta t L_3^n)(\phi^{***}-\phi^n) = \phi^{**}-\phi^n \tag{5c}$$

$$\phi^{n+1} = \phi^{***} + O(\Delta t^3) \tag{5d}$$

If spatial derivatives appearing in L are replaced by three-point difference formulas, then each step in Eqs. (5a-c) can be solved by a block-tridaigonal "inversion". Eliminating the intermediate steps in Eqs. (5a-d) results in

$$(I-\beta\Delta t L_1^n)(I-\beta\Delta t L_2^n)(I-\beta\Delta t L_3^n)(\phi^{n+1}-\phi^n) = \Delta t D(\phi^n) \tag{6}$$

which approximates Eq. (4) to order Δt^3. Complete derivations are given by the authors in [7, 8]. It is noted that Beam & Warming [10] have reformulated this algorithm as a widely-used "delta form" approximate factorization scheme whose two-level form is identical to Eq. (5).

MESH REFINEMENT IN TWO AND THREE DIMENSIONS

Solutions were computed for three-dimensional horseshoe vortex flow past an elliptical leading edge for free stream angle of incidence α of zero and five degrees. These solutions have the following flow parameters: 5:1 ellipse, chordal Reynolds number of 400, Mach number 0.2, and flat plate leading edge located 1.25 chords upstream of the leading edge of the ellipse. For reasons of economy, these solutions were computed using a coarse computational grid, the finest being 14x28x14 (ξ,η,z) for $\alpha=5^o$. However, the geometry, flow conditions, and grid distributions were carefully adjusted to provide the best resolution possible within this constraint. Most length scales expected to be present in this type of flow receive at least modest resolution. Specifically, care was taken to provide resolution of boundary layers on the endwall and ellipse, of the Heimenz layer at the leading edge stagnation point, and of the flow region within one leading edge radius of both the leading edge and the endwall. The only potentially-relevant unresolved length scale is an $O(Re^{-3/8})$ streamwise distance predicted by two-dimensional "triple deck" theory near a separation point.

The truncation error associated with the present flow and computational grid was examined by mesh refinement and by comparison with an incompressible solution of Lugt and Ohring [11] for two-dimensional flow past a 10:1 ellipse at zero incidence and Re=200. The latter comparison for streamwise velocity at the present outflow boundary ($\eta=\pi/2$) is shown in Fig. 2. The agreement is quite reassuring in light of the respective differencing procedures and meshes. Good agreement was also obtained for surface pressure distributions. Additional two-dimensional solutions for the forward half of a 5:1 ellipse ($\alpha=0^o$, Re=200, η=0.2) were computed assuming symmetry about the chord line $\eta=\pi$ and using both 14x14 and 28x28 grids. The streamwise velocity U along the stagnation streamline is a sensitive indicator of mesh dependence and is shown on a logarithmic scale in Fig. 3. The 14x14 mesh is identical to the 14x28 mesh used for ξ,η in the three-dimensional solutions without symmetry about $\eta=\pi$, and the small amount of mesh dependence in Fig. 3 indicates that this mesh should be adequate, at least away from the endwall. Finally, resolution normal to the endwall (z direction) was examined for three-dimensional flow at 5^o incidence using both 14x28x10 and 14x28x14 grids. The velocity profile at x=-1.06, y=0 near separation is the most sensitive indicator and is shown in Fig. 4. The finer mesh improves resolution considerably very near the endwall flow reversal, but makes little difference elsewhere.

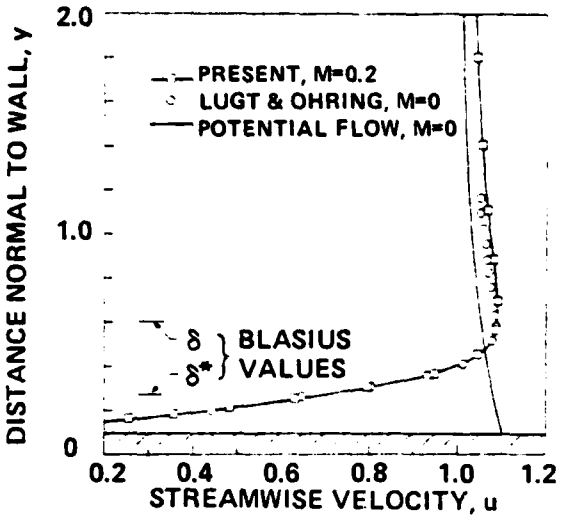

Fig. 2 - Velocity Profiles at Outflow Boundary ($\eta=\pi/2$) for 10:1 Ellipse, $\alpha=0^{o}$, Re=200.

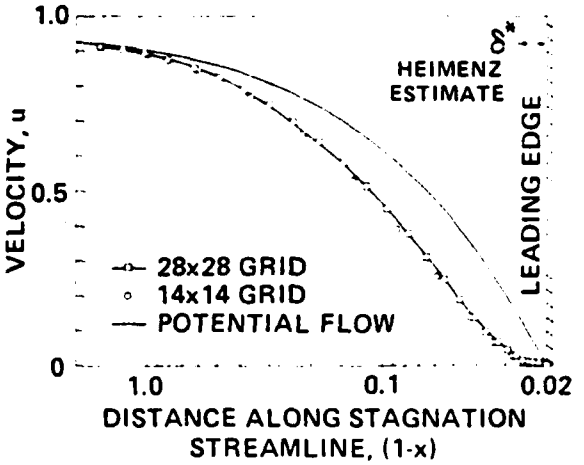

Fig. 3 - Velocity Along Stagnation Streamline ($\eta=\pi$) for 5:1 Ellipse, $\alpha=0^{o}$, Re=400

The foregoing results provide a limited but informative assessment of truncation error associated with the present calculations. The solutions may be characterized as having both qualitative significance and reasonable quantitative accuracy. Any potential concern that failure to provide high resolution near separation would cause serious error (beyond a local smoothing of the flow) may be unwarranted in light of these resolution tests.

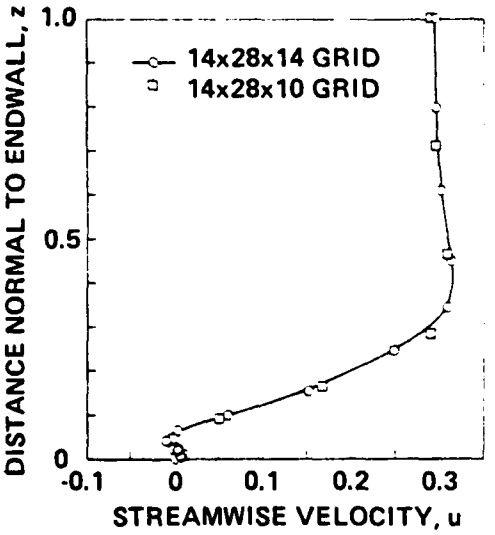

Fig. 4 - Streamwise Velocity Profiles Near Separation for 5:1 Ellipse, $\alpha=5^{o}$, Re=400.

HORSESHOE VORTEX FLOW

Representative results from solutions for three-dimensional horseshoe vortex flow at zero and five degree incidence are shown in Figs. 5a-f. These solutions converged in about 80 time step iterations and with a 14x28x14 grid ($\alpha=5^{o}$) required about 20 minutes of CDC 7600 run time. A 14x28x10 grid was used for $\alpha=0^{o}$. In Figs. 5a-b, vector plots of velocity in a plane one grid point away from the no-slip endwall surface are shown. Here, a saddle-point type of flow separation is evident upstream of the leading edge and, in the case of $\alpha=5^{o}$, toward the (upper) high pressure surface of the ellipse. The remaining plots in Fig. 5 show flow velocities in the plane z=0.15, located approximately in the center of both the horseshoe vortex flow region and the approaching boundary layer. Here, the velocity vector plots are not much different from the two-dimensional flow region near z=1 (not shown), and the most significant feature of the flow is seen in the contours of velocity normal to the endwall (and to the page) in Figs. 5e-f. A strong downward flow toward the endwall is present near the leading edge (behind the saddle-point separation), with maximum downward velocity of 28 percent of the freestream reference velocity for $\alpha=0^{o}$ and 32 percent for $\alpha=5^{o}$. Further results for $\alpha=5^{o}$ are shown in Figs. 6a-f.

Contours of total pressure loss coefficient $\Delta p_o/(\rho_r U_r^2/2)$ for z=0.15 are shown in

Fig. 6a. In Fig. 6b, the velocity in the stagnation plane normal to and containing the ellipse leading edge again shows the strong downward flow toward the endwall near the leading edge. The cross-flow velocity in outflow planes is shown in Figs. 6c-d. A moderately strong secondary flow pattern (peak velocity 20% of u_r) indicative of a streamwise corner vortex is clearly in evidence near the suction surface in Fig. 6d. Finally, a "limiting" surface velocity vector plot and contours of pressure coefficient are shwon in Figs. 6e-f for the surface one grid point away from the surface of the ellipse ("unwrapped" to lie in a plane). Here there is evidence of the distorted stagnation line near the endwall, flow toward the endwall near the stagnation line, and finally the formation of a streamwise vortex visible mainly on the low pressure or suction surface near the endwall.

CONCLUDING REMARKS

Although no other analytical results or experimental measurements of the three-dimensional horseshoe vortex flow are available for comparison, the present computed results are consistent with flow visualization studies of related leading edge vortex flows. Computed results in three dimensions have illuminated several aspects of the flow structure. For flows having nontrivial endwall boundary layer development upstream of the leading edge, the horseshoe vortex structure consists of an inertially-dominated rotational flow except very near the solid boundaries, where viscous effects occur within thin layers generated locally by the leading edge interaction. The rotational inviscid portion of the vortex structure both upstream of the leading edge and in the downstream corner flow region scales with the approaching endwall boundary layer thickness. Viscous effects are confined to thin regions near the surfaces, having a thickness which is apparently not strongly dependent on the approaching boundary layer. The overall flow consists of a saddle-type flow separation on the endwall upstream of the leading edge, a strong spanwise flow toward the endwall near the leading edge, and streamwise vortices in the corner region downstream of the leading edge. The strength of the streamwise corner vortex is significantly increased on the suction surface corner for flow at nonzero incidence. Regarding the present use of "zone embedding" and interactive boundary conditions to minimize the computed flow region, the general conclusion is that while boundary conditions cannot be treated with complete rigor when located within an elliptic region of nonuniform flow, careful treatment can lead to quite reasonable results which appear completely adequate for the present goal of horseshoe vortex analysis.

ACKNOWLEDGMENT

This work was supported by the Office of Naval Research.

REFERENCES

1. Belik, L., Aero. Quart., Feb. 1973, p. 47.
2. Baker, C. J., J. Fluid Mech., 95, 1979, p. 347.
3. Barber, T. J., J. Aircraft, 15, 1978, p. 676.
4. Dwyer, H. A., AIAA Paper No. 68-740, 1968.
5. Hawthorne, W. R., J. Aero. Sci., 21, 1954, p. 588.
6. Milne-Thomson, L. M., Theoretical Hydrodynamics, Macmillan Co., New York, 1960, p. 164.
7. Briley, W. R. and McDonald, H., J. Comp. Physics, 24, 1977, p. 372.
8. Briley, W. R. and McDonald, H., J. Comp. Physics, 34, 1980, p. 54.
9. Douglas, J. and Gunn, J. E., Numer. Math., 6, 1964, p. 428.
10. Beam, R. M. and Warming, R. F., AIAA Journal, 16, 1978, p. 393.
11. Lugt, H. J. and Ohring, S., Physics of Fluids, 18, 1975, p. 1.

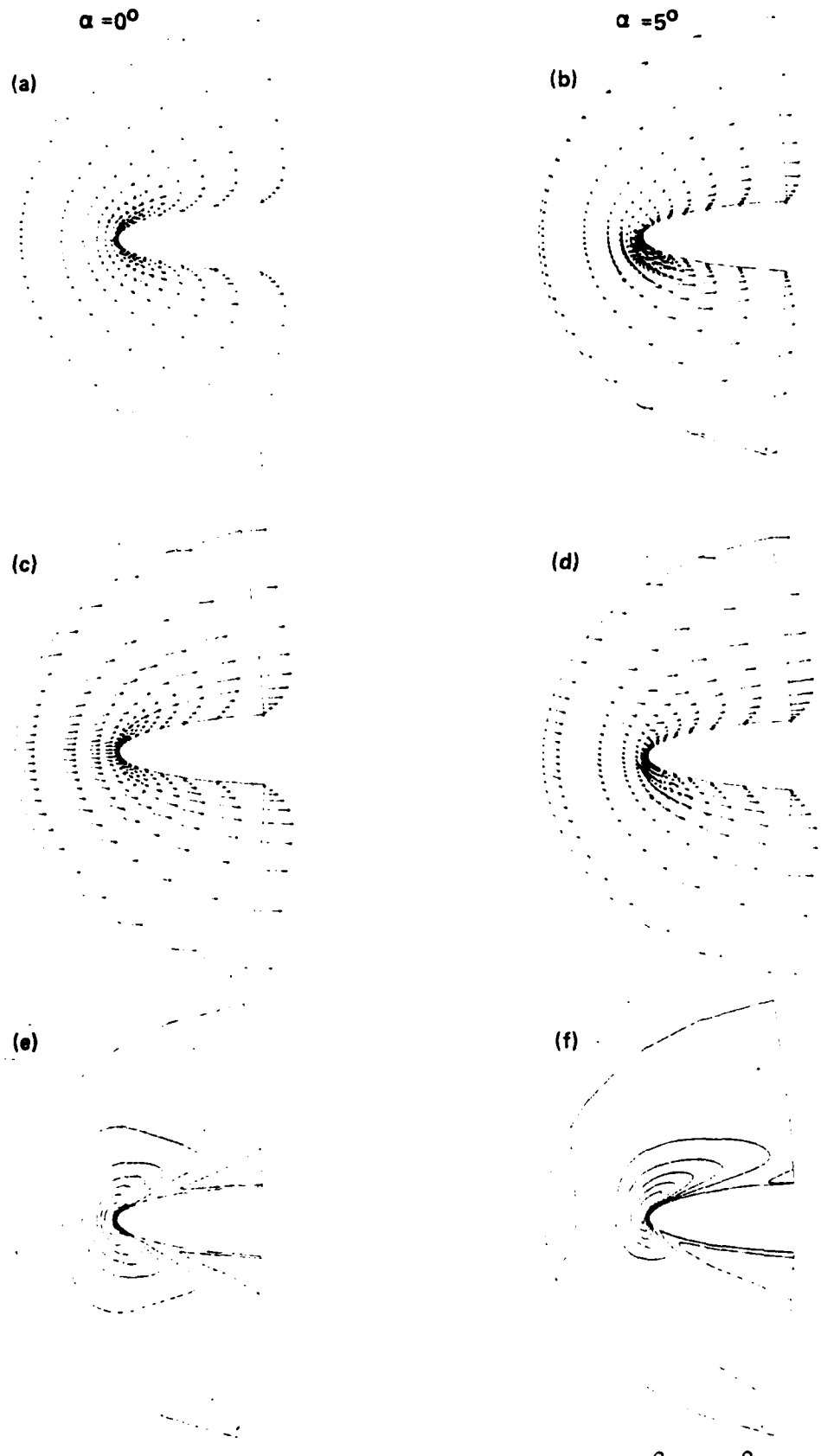

Fig. 5 - Detail of Computed Velocity for 5:1 Ellipse with $\alpha=0^{\circ}$ and 5°, Re=400, M=0.2. (a,b): the plane of grid points adjacent to endwall surface; (c,d): the plane z=0.15 (near center of approaching boundary layer); (e,f): contours of velocity w normal to endwall in the plane z=0.15.

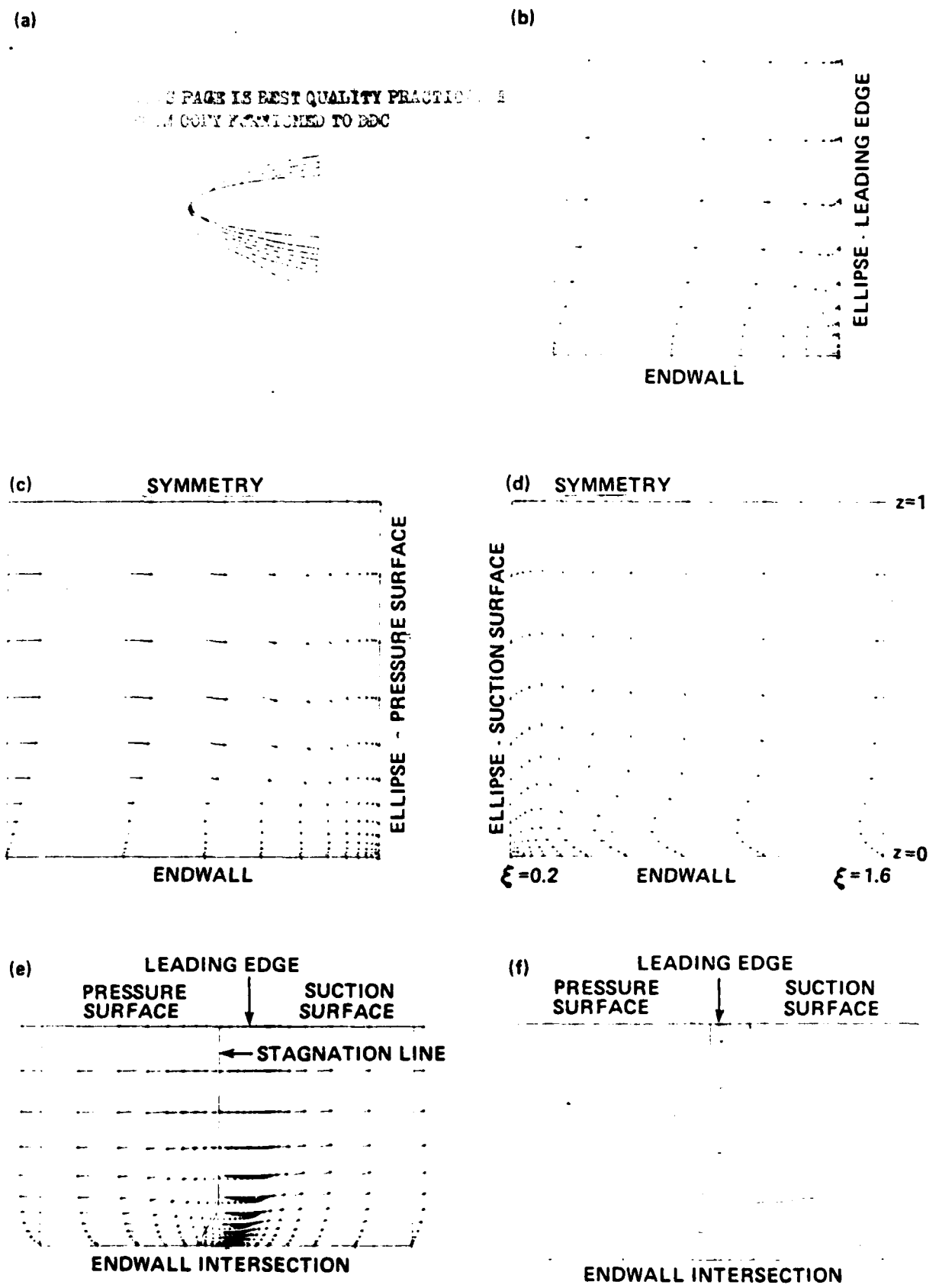

Fig. 6 - Detail of Horseshoe Vortex Flow for 5:1 Ellipse with $\alpha=5^{\circ}$, Re=400, M=0.2. (a)-Total pressure loss coefficient in z=0.15 plane; (b)-Velocity in plane containing leading edge; (c,d)-Secondary velocity in outflow surfaces; (e,f)-Velocity and contours of pressure coefficient in "unwrapped" surface of points adjacent to ellipse.